metals

MDPI

Article

Microstructure and Mechanical Properties of Friction Welding Joints with Dissimilar Titanium Alloys

Yingping Ji [1,2], Sujun Wu [2,*] and Dalong Zhao [2]

[1] School of Mechanical Engineering, Ningbo University of Technology, Ningbo 315211, China; yingping04@163.com

[2] School of Materials Science and Engineering, Beihang University, Beijing 100191, China; zhaodalong_buaa@126.com

* Correspondence: wusj@buaa.edu.cn; Tel.: +86-10-8231-6326

Academic Editor: Giuseppe Casalino

Received: 5 April 2016; Accepted: 5 May 2016; Published: 10 May 2016

Abstract: Titanium alloys, which are important in aerospace application, offer different properties via changing alloys. As design complexity and service demands increase, dissimilar welding of the titanium alloys becomes a particular interest. Linear friction welding (LFW) is a relatively novel bond technique and has been successfully applied for joining titanium alloys. In this paper, dissimilar joints with Ti-6Al-4V and Ti-5Al-2Sn-2Zr-4Mo-4Cr alloys were produced by LFW process. Microstructure was studied via optical microscopy and scanning electron microscopy (SEM), while the chemical composition across the welded samples was identified by energy dispersive X-ray spectroscopy. Mechanical tests were performed on welded samples to study the joint mechanical properties and fracture characteristics. SEM was carried out on the fracture surface to reveal their fracture modes. A significant microstructural change with fine re-crystallization grains in the weld zone (WZ) and small recrystallized grains in the thermo-mechanically affected zone on the Ti-6Al-4V side was discovered in the dissimilar joint. A characteristic asymmetrical microhardness profile with a maximum in the WZ was observed. Tensile properties of the dissimilar joint were comparable to the base metals, but the impact toughness exhibited a lower value.

Keywords: dissimilar friction weld; titanium alloy; evolution of microstructure; mechanical property

1. Introduction

Dissimilar weld is attracting increasing attention because it can take advantage of specific attributes of each material to enhance the performance of a product or introduce new functionalities. They are applied in various fields such as thermal power station, nuclear industries, automobile, aerospace, *etc.* A number of dissimilar joints with aluminum, titanium, ferrous and many kinds of materials have been successfully formed by various methods from fusion welding to friction welding process [1–5].

With high strength to weight ratio, corrosion resistance, and good strength sustainability at high temperatures, titanium alloys are important in aerospace applications. As design complexity and service demands increase, dissimilar welds with titanium alloys become a particular interest in the field of aerospace industry [3–5]. There have been a number of studies reporting the welding of dissimilar titanium alloys using various different welding processes, including friction stir welding [3], ultrasonic spot welding [4], linear friction welding (LFW) [5,6], tungsten inert gas welding [7] and electron beam welding [8].

LFW is a relatively novel solid-state joining process where two metals are welded together under reciprocating motion and apply force against each other [9]. Compared with traditional fusion welding technologies, LFW has many advantages such as less defect formation and the ability to join dissimilar

materials and complex geometrical components, and it often negates the need for protective gas [10]. To date, LFW has been successfully used to join titanium alloys [9–12], nickel-base alloys [13,14] as well as other materials [15–17]. More importantly, the process can be viable for the production of dissimilar welds. For example, Bhamji *et al*. applied LFW process successfully to join aluminum and copper. The welds had good electrical and mechanical properties [18]. They also joined an aluminum alloy to a magnesium alloy by LFW and found that these welds had a reasonable strength [19]. Ma *et al.* produced a dissimilar Ti-6Al-4V and Ti-6.5Al-3.5Mo-1.5Zr-0.3Si joint by LFW and identified the microstructural evolution of the joint. They found different microstructure zones such as the TMAZs and weld zones in both sides of base metals. In addition, they investigated the mechanical properties and found the tensile strength of the joint was comparable to that of the parent [20]. Wen *et al.* made LFW dissimilar joints of Ti-6Al-4V and Ti-6.5Al-3.5Mo-1.5Zr-0.3Si and evaluated the microstructure, microhardness, and fatigue properties of the joint, which had essentially symmetrical hysteresis loops and an equivalent fatigue life to the base metals [21]. Zhao *et al*. investigated the influence of strain rate on the tensile properties of LFW dissimilar joints between Ti-6.5Al-3.5Mo-1.5Zr-0.3Si and Ti-4Mo-4Cr-5Al-2Sn-2Zr titanium alloys [22]. Frankel *et al.* compared the residual stresses between Ti-6Al-4V and Ti-6Al-2Sn-4Zr-2Mo [23].

Although LFW is a promising process for joining dissimilar titanium alloys, there are only a few public papers on this subject [20–23]. There are a great many publications about the LFW process for same titanium alloy. Karadge *et al.* detailed the texture of LFW Ti-6Al-4V joints by experiment [24]. Microstructural evolution of LFW Ti-6.5Al-3.5Mo-1.5Zr-0.3Si joint [25], the relationship between forging pressure and the microstructure of LFW Ti-6Al-4V joint were also revealed [26]. Interrelationship of microstructure and mechanical properties of LFW titanium joint was also investigated [27]. In addition, to predicting various weld responses, such as thermal fields and microstructural evolution, a great number of finite element models were established and the predictions of the models were found to be in good agreement with the experimental results [28–31].

These investigations on LFW joints with dissimilar and similar materials show that the microstructure and property can be established for given LFW joints through extensive experiments. However, due to the complicated nature of interaction between the LFW thermomechanical environment and the material microstructure, these findings cannot be easily extended to other LFW joints. Consequently, to expand the application of LFW process in dissimilar titanium alloy, it is necessary to investigate LFW joint with Ti-6Al-4V (Ti64) and Ti-5Al-2Sn-2Zr-4Mo-4Cr (Ti17). In this paper, two different titanium alloys consisting of one α + β alloy Ti64, and one near-β alloy Ti17, were welded by LFW process. The present study was focused on revealing the micro-structural characterization, mechanical properties, as well as the fracture mode of the dissimilar joints.

2. Materials and Methods

The base metals for the LFW process are Ti64 and Ti17 alloys, whose nominal chemical compositions are listed in Table 1.

Table 1. Chemical compositions of base metals (wt. %).

Alloy	Al	V	Sn	Zr	Mo	Cr	Fe	Si	C	N	H	O	Ti
Ti64	6.06	3.93	-	-	-	-	0.103	0.15	0.106	0.033	0.015	0.13	Balance
Ti17	5.05	-	2.13	2.07	4.12	4.13	0.30	-	0.05	0.05	0.013	0.08	Balance

The typical microstructures of the as-received materials revealed by scanning electron microscopy (SEM) are shown in Figure 1. SEM analysis was performed on an Apollo 300 (Camscan, Cambridge, UK). As shown in Figure 1a, Ti64 alloy is characterized by typical bimodal microstructure with globular primary α (α_p) distributed in the matrix of transformed β (β_t). The prior β grain size is 10–15 μm and the α_p size is about 20 μm. Ti17 alloy has a typical lamellar structure with lath α_p in 10–30 μm length and fine secondary α (α_s) embedded in β phases (Figure 1b).

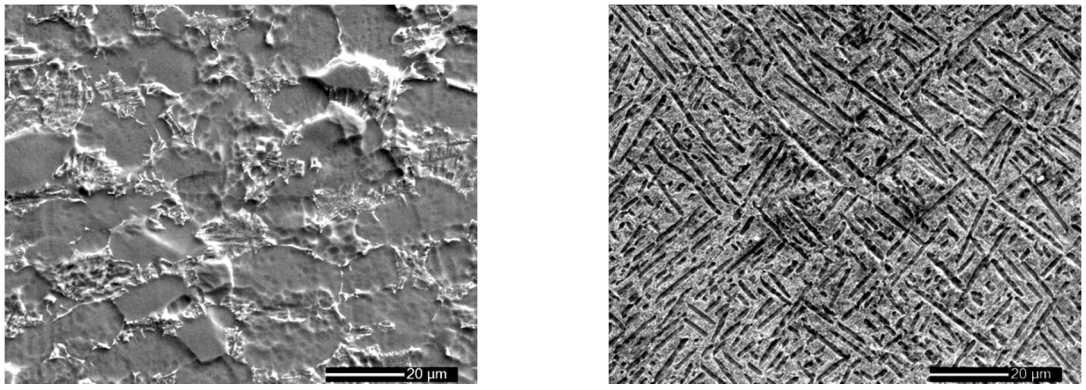

(**a**) (**b**)

Figure 1. Microstructure of base metals: (**a**) Ti64 and (**b**) Ti17.

Attempts were made to weld samples of geometry 130 × 75 × 20 mm with a weld interface of 75 × 20 mm. Ti64 and Ti17 titanium alloys were used for the dissimilar LFW trials. Welds were produced on a homemade linear friction welding machine of LFW-20T. The Ti64 sample was reciprocated, while the Ti17 sample was held stationary. Prior to welding, the welding surfaces of the samples were ground and cleaned in an acetone bath. The welding parameters were selected as follows: amplitude of oscillation of 3 mm, frequency of oscillation of 50 Hz, friction force of 4.8 kN and friction time of 3 s. Post weld heat treatment was carried out at 630 °C for 3 h in vacuum to relieve residual stress. The welded specimens for investigation were free from surface defects and internal defects.

The LFW specimens for micro-structural observation were cut perpendicularly to the reciprocating motion direction and prepared by standard procedures followed being etched with Kroll's reagent (2 mL concentrated nitric acid, 1 mL hydrofluoric acid and 5 mL distilled water). Microstructure was investigated by light optical microscopy (OM, Olympus, Tokyo, Japan) and SEM. Energy dispersive X-rays (EDS, Kratos Analytical Ltd, Manchester, UK) was applied to analyze the compositional change across the welds.

Mechanical property studies included Vicker's micro-hardness tests, tensile tests and U notch impact toughness tests. Vickers micro-hardness tests were performed with a load of 500 g and a dwell time of 15 s. Tensile tests were carried out at room temperature in accordance with GB/6397-86 (China), using a fully computerized tensile testing machine at constant strain rates of 10^{-4} m·s^{-1}. A drop hammer impact testing machine was used to measure the impact toughness of specimens, which was performed according to GB/T229-1994 (China). For comparison, base material specimens were tested and had the same overall dimensions as those for the welded. For a given variant, at least three specimens were tested.

To ensure the center of U-notch located in the center of weld zone, the weldments for impact tests were polished on one side and etched by a Kroll's reagent before machining the U-notch. The configuration and size of specimens for tensile and impact tests are shown in Figure 2a,b, respectively.

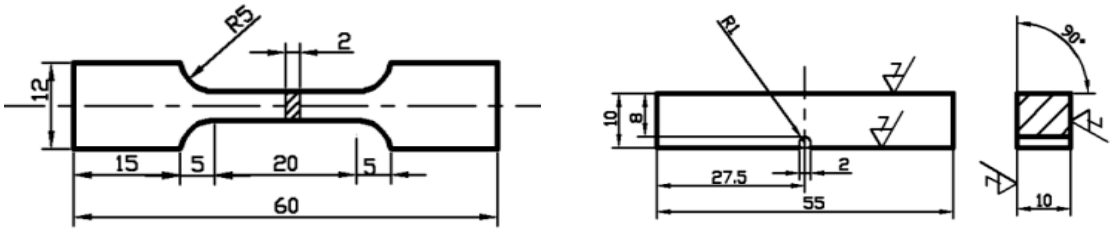

(**a**) (**b**)

Figure 2. Configurations of specimens for (**a**) tensile and (**b**) impact toughness tests.

3. Results and Discussion

3.1. Macro and Microstructure

A low magnification overview of a dissimilar LFW joint using OM is presented in Figure 3. The weld interface appearing wavy is obvious between two base metals. On both sides, the microstructure shows a gradual change from the weld interface towards the base metals, but a less gradual micro-structural transition and smaller region with elongated grains is observed in the side of Ti17 than Ti64. According to the micro-structural characteristics, welded joints could be divided into four zones: weld zone (WZ), thermo-mechanically affected zone (TMAZ), heat affected zone (HAZ) and base metals (BM). Faint indications of grain boundaries are seen, but, overall, the grains along the weld center are not effectively revealed. To reveal the details of the weld microstructure, the corresponding SEM images of different zones at high magnification are provided in Figure 4.

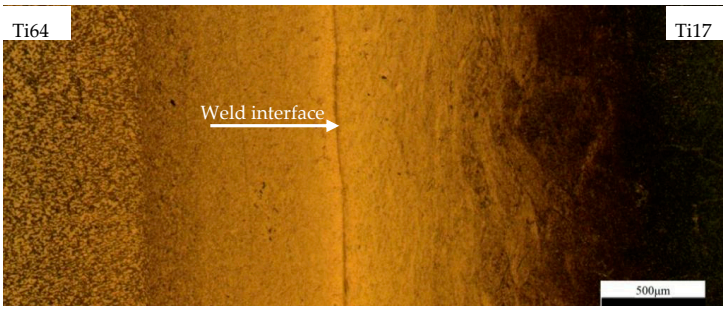

Figure 3. Cross section of the linear friction welding (LFW) joints with Ti64 and Ti17 alloys.

As shown in Figure 4a, in the HAZ of Ti64 side (Ti64-HAZ), an un-deformed bimodal microstructure that is characteristic of the base metal Ti64 (Figure 1a) can be observed clearly. However, the image of α_s in β_t becomes less clear while the shape of α_p remains unchanged, suggesting that the dissolution of the α_s occurred in this region during welding. With the decreasing distance to the weld center, the thermo-mechanically affected zone of Ti64 (Ti64-TMAZ) with severe plastic deformation is observed, where the α_p are elongated and the residual β are reoriented along the oscillation direction. In addition, some necklace-shaped microstructures distributed along the grain boundaries of deformed grains are also observed in this region (Figure 4b). This indicates that partially re-crystallization occurred to Ti64-TMAZ adjacent to weld center during the LFW process. Unlike HAZ and TMAZ, WZ has completely different microstructures, which consists of fully re-crystallized grains with fine size around 20 μm (Figure 4c). In the case of microstructures in the Ti17 side, they are similar to those in the Ti64 side. As shown in Figure 4d,e, grains are elongated and reoriented with their long dimension perpendicular to the applied force in the thermo-mechanically affected zone of Ti17 (Ti17-TMAZ) while some retention and annihilation of the Ti17 microstructures are observed in heat affected zone of Ti17 (Ti17-HAZ).

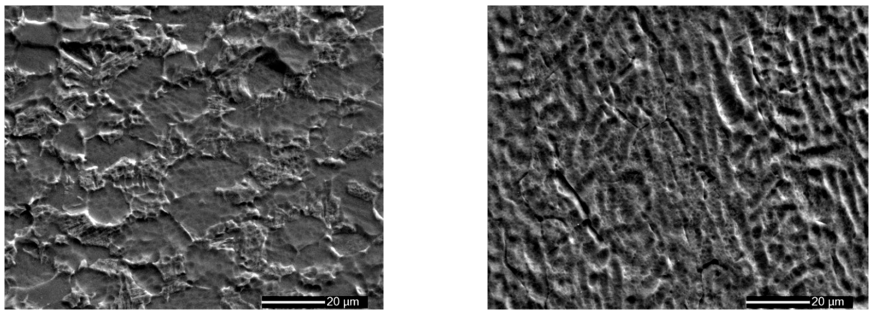

(**a**) (**b**)

Figure 4. *Cont.*

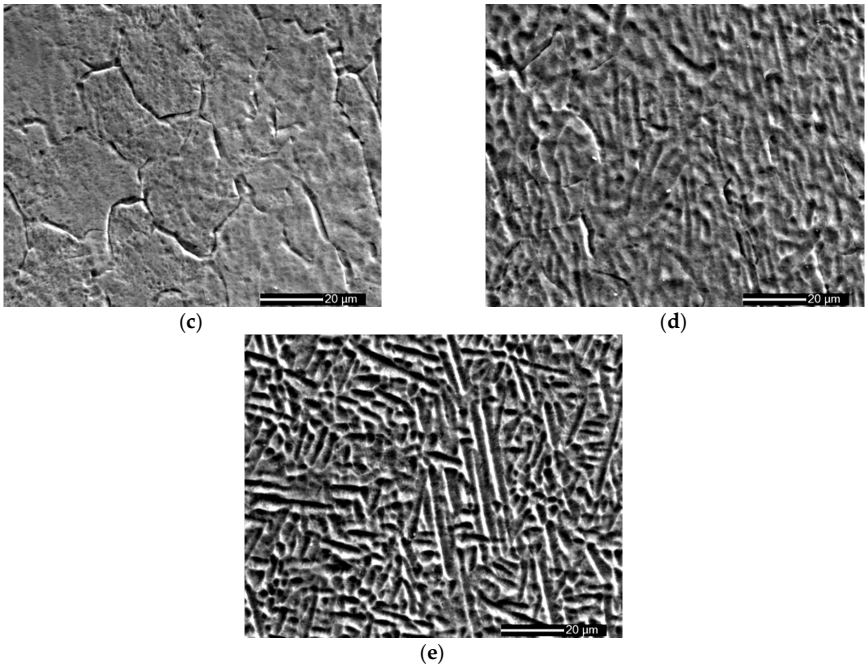

(**c**) (**d**)

(**e**)

Figure 4. Typical microscopic structures across a friction welded joint with Ti64 and Ti17 alloys: (**a**) Ti64-heat affected zone (HAZ); (**b**) Ti64-thermo-mechanically affected zone (TMAZ); (**c**) weld zone (WZ); (**d**) Ti17-TMAZ and (**e**) Ti17-HAZ.

As described in the above section, a significant micro-structural change is observed across the dissimilar joints. The gradient of temperatures and strains along the joints attribute to the difference. During LFW process, WZ simultaneously underwent serious plastic deformation and sufficient frictional heat due to the linear movement influenced by friction and upset pressures, where temperatures above the β-transus (β_t) point [32,33]. This plastic deformation introduced a large number of dislocations in the materials of welding interface. As the density of these dislocations increased, they tended to form sub-grain cell structures. These low-angle grains rotated to form high-angle strains free grains, resulting in very fine equal-axed grains in WZ. In the case of materials in the TMAZ, they experienced thermo-mechanical deformation in sub β_t temperature [33,34] and the deformation was in a smaller extent, so there was no sufficient deformed energy to fully activate re-crystallization and the part re-crystallization occurred to the deformed grain boundaries. In the case of HAZ, a little heat was conducted from the WZ to the zone, leading to the dissolution of α_s.

3.2. Compositional Analysis

A line scan EDS profile across the weld interface (scan in Figure 5a) is shown in Figure 5b. It clearly shows the existence of a mixed layer at the interface with a composition between that of Ti64 and Ti17. The composition abruptly changes at the Ti64 interface while the transition is more gradual on the Ti17 side of the joint. It indicates that the dissimilar welds had a compositional heterogeneity and element diffusion occurred to Ti64 and Ti17 during LFW process. For example, a significant diffusion of V (The curve with red colure) into Ti17 side is obvious. However, no long range inter-diffusion crossing the interface could be observed, which is in agreement with the study on LFW of Ti-6Al-4V and Ti-6Al-2Sn-4Zr-6Mo [10]. This may be related to the limited atomic diffusion resulting from the short time above the βt temperature during the LFW process.

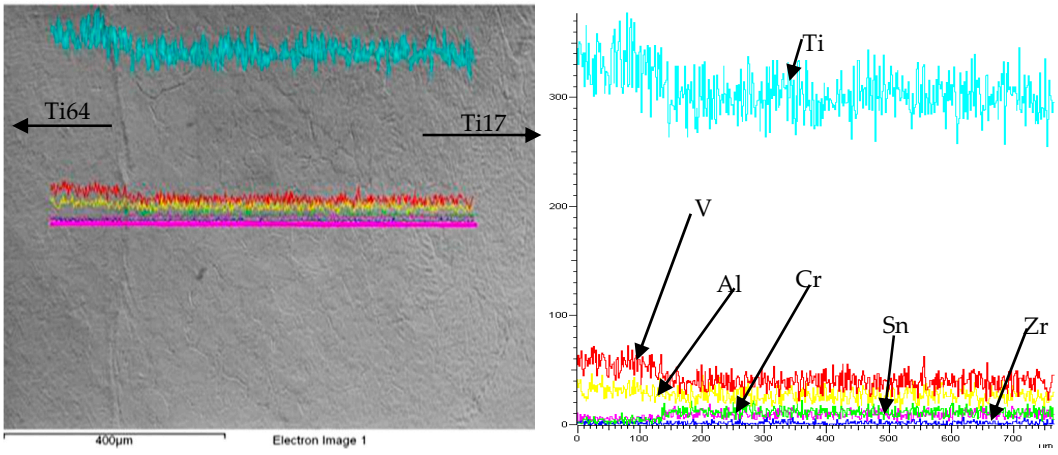

Figure 5. (**a**) SEM micrograph of LFW joints with Ti64 and Ti17 alloys and (**b**) the corresponding SEM-EDS line scans across the interface.

3.3. Microhardness

The microhardness across the weld interface of dissimilar LFW joints is presented in Figure 6. An asymmetrical microhardness profile across the weld is obvious with an average value of 332 HV for Ti64 and approximately 350 HV for Ti17, respectively. In addition, a distinct increase from each base metal up to the weld interface is also observed and a maximum of 420 HV occurs to WZ. The micro-hardness development in the LFW joints with dissimilar Ti64 and Ti17 alloys is similar to what has been reported in the literature studied on LFW joints with titanium alloys [33]. The increase in hardness of WZ could be ascribed to the grain refinement resulted from dynamic re-crystallization. It is expected that the high hardness within the WZ is going to influence the fracture properties of the welds.

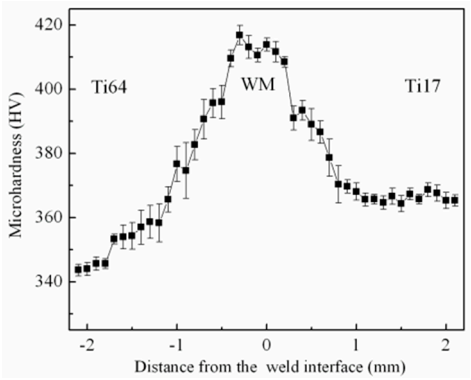

Figure 6. Transverse hardness of LFW joints with Ti64 and Ti17 alloys.

3.4. Tensile Properties

The average tensile properties of four LFW joints are given in Table 2. For a comparison, the tensile properties of base metals Ti64 and Ti17 are also included, where the values are the mean of three specimens for each base metal. For base metals, Ti64 has yield strength (YS) of 838 MPa, ultimate tensile strength (UTS) of 904 MPa and ductility of 14.6%, while Ti17 has higher strength and lower ductility. The higher strength of Ti17 than Ti64 is responsible for the smaller width of Ti17-TMAZ than Ti64-TMAZ as presented in Figure 3. In the case of LFW joints, they show a superior strength and lower ductility than base metal Ti64, but exhibit a contrary trend compared with base metal Ti17.

It should be stated that the failure of LFW specimens in the tensile tests located in the Ti64 side, approximately 1.2 mm away from the welding interface. It suggests that a highly durable and sound dissimilar joint of Ti64 and Ti17 was achieved via LFW process. The phenomenon was also observed in the tensile and fatigue tests on dissimilar LFW joints of Ti-6Al-4V to Ti-6.5Al-3.5Mo-1.5Zr-0.3Si [20,21]. This may be resulting from the lower strength of Ti64 and the reaction zone formed at Ti64 side. Firstly, compared with the regions of Ti17 side close to the interface, the regions in the Ti64 side had lower hardness and strength, where cracks were apt to initiate. Secondly, a reaction zone with equi-axil grains formed in Ti64 side, this would be the weakest zone for the crack to initiate. However, further work is still needed to clearly reveal this phenomenon.

Table 2. Tensile properties of base metals and joints.

Specimen	UTS/MPa	YS/MPa	Elongation δ%
Ti64	904	838	14.6
Ti64/Ti17 Joints	950	888	11.9
Ti17	1134	1044	10.6

The tensile fracture surfaces exhibited in Figure 7 indicate that all specimens crack in a ductile mode. It is evident that the dimples on the surface of dissimilar welds are in globular shaped (Figure 7b), which are similar to that on the fracture surface of base metal Ti64 (Figure 7a). This resulted from the fact that the failure of welding joints occurred in the zone of Ti64 side. In the case of Ti17, the dimples are strip-shaped (Figure 7c), which are smaller and shallower than those on the surface of Ti64 and joints, corresponding to the smaller elongation.

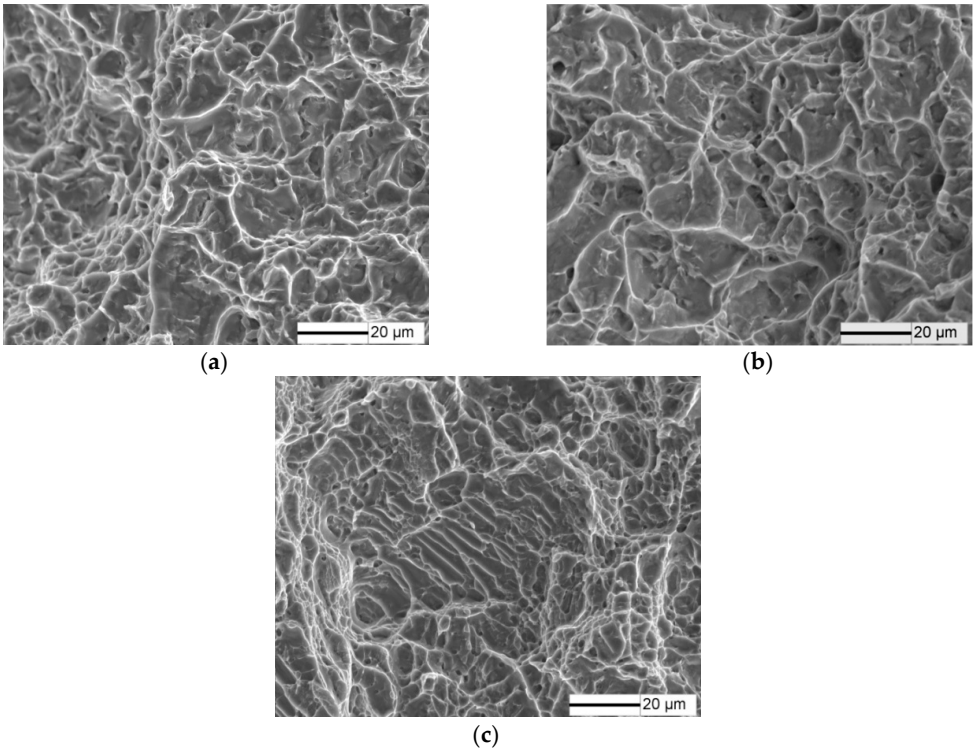

Figure 7. Fracture surface of (**a**) Ti64; (**b**) joints and (**c**) Ti17.

3.5. Impact Toughness

The impact toughness is characterized by a_k, a value defined through dividing the impact energy by the minimum cross-sectional area of the starting sample [35]. The impact toughness of joints and

base metals are shown in Table 3, which are the average values of three specimens for the given variant. It is found that Ti17 has superior impact toughness than Ti64. In addition, WZ presents a lower toughness than base metals with an average value about 38.7 J/cm^2. This is in disagreement with the previous research on impact toughness of linear friction welded Ti-6Al-4V alloy joints, where the impact toughness of the weld was higher than that of the base metal Ti-6Al-4V [35].

Table 3. Impact toughness of WZ and base metals.

Sample	Ti64	WZ	Ti17
a_k (J/cm^2)	44.5	38.7	53.6

The corresponding fracture surfaces of impact toughness specimens are shown in Figure 8. It is obvious that the fracture surfaces of base metals both show trans-granular fracture mode (Figure 8a,c), which are similar to that of tensile tests. In contrast to base metals, some small dimples and facts corresponding with the fine grains are shown in WZ (Figure 8b), suggesting that a mixture failure mode of trans-granular coupled with inter-granular occurred in WZ. Failure in the inter-granular mode that occurred in the WZ of LFW joint was also observed in fracture toughness tests [36].

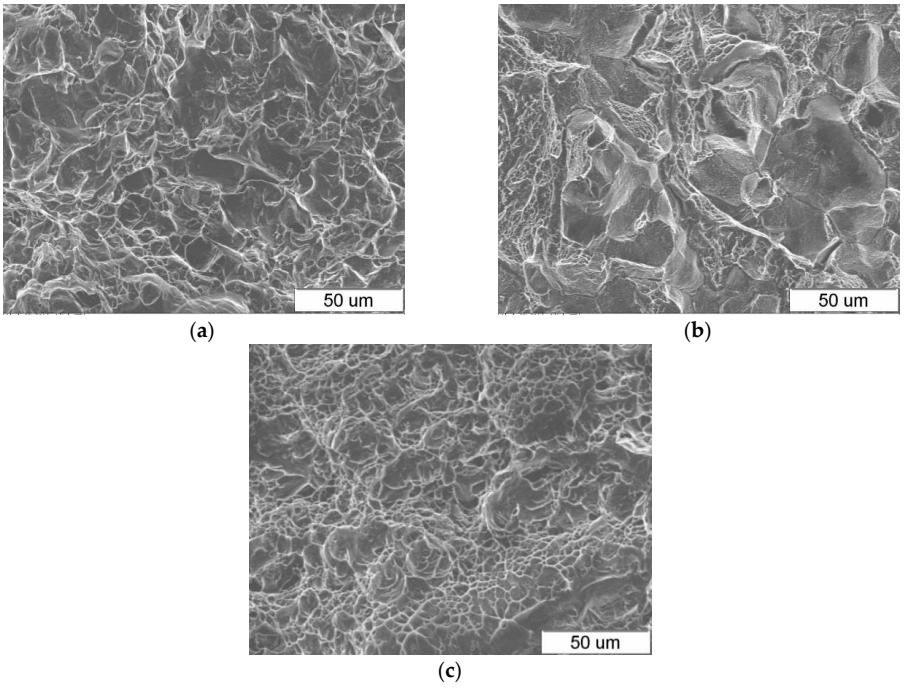

Figure 8. The typical fracture surface of (**a**) Ti64; (**b**) WZ and (**c**) Ti17.

For base metals, Ti17 alloy shows a higher toughness than Ti64 alloy, which results from the microstructures. On the one hand, the boundaries of α_p are the preferred sites for micro-crack nucleation and provide a relatively easy path for fracture propagation. Therefore, with a decreased fraction of α_p, the nucleation sites of micro-cracks in Ti17 alloy at the α_p phase decreased, leading to superior impact toughness than Ti64. On the other hand, the crack path is apt to deflect at grain boundaries, colony boundaries, or arrested and deviates at α/β interface in titanium alloys, which consumes more of the plasticity energy path and results in improved toughness. In the present test, the lamellar microstructure with more colony boundaries displayed a more tortuous and deflected crack path than the bimodal microstructure, leading to the superior toughness of Ti17 alloy.

It is unexpected that a marginally lower toughness occurred for WZ with superfine microstructures in the present research. The significant decrease of impact toughness in WZ could be

related to a combination of factors. Firstly, the soft phase of continuous α layer that lined the prior β grain boundary was effectively less constrained by the harder surrounding intra-granular structure, leading to the inter-granular failure and degradation of toughness. Secondly, with high oxidation tendency, it is inevitable that the titanium alloy oxidation takes place during the friction weld process, even though most of the oxide layer was expelled from the friction surface during the welding process. Some of the nano-scale oxides, however, could be left in the weld joints, and segregated in the fine grain boundaries during re-crystallization, resulting in the weakened grain boundaries in the WZ. This attributes to a further degradation of the toughness of WZ.

4. Conclusions

The micro-structural evolution, micro-hardness, tensile properties and impact toughness of LFW dissimilar welds with Ti64 and Ti17 alloys were investigated. The following conclusions were drawn.

(1) The microstructure across the linear friction welding dissimilar joints with titanium alloys displayed marked change, mainly consisting of a re-crystallized grain zone in the weld center, deformed grains and partial re-crystallization in the thermo-mechanical affected zones, and dissolved secondary α in the heat affected zones.

(2) The maximum hardness is located in the weld metal, which may result from the fine grains arising from the rapid cooling during the welding process.

(3) The linear friction welding dissimilar joints obtained higher tensile strength than base metal Ti64 with lower strength. The failure located in the Ti64 side approximately 1.2 mm away from the welding interface.

(4) Base metals had superior impact toughness and fractured in a trans-granular mode, but weld zone exhibited decreased toughness and failed in a mixture of trans-granular and inter-granular fracture modes.

Acknowledgments: This work has been financially supported by "Fracture Mechanism of Dissimilar Titanium Alloy Welded Joints" Ningbo Natural Science Foundation program (No. 2015A610071). As part of these grants, we received funds for covering the costs to publish in open access.

Author Contributions: Yingping Ji and Sujun Wu conceived and designed the experiments; Yingping Ji and Dalong Zhao performed the experiments; Yingping Ji analyzed the data; Yingping Ji and Sujun Wu contributed to writing and editing the manuscript.

Conflicts of Interest: The authors declare no conflict of interest.

References

1. Mvola, B.; Kah, P.; Martikainen, J. Dissimilar ferrous metal welding using advanced gas metal arc welding processes. *Rev. Adv. Mater. Sci.* **2014**, *38*, 125–137.
2. Martinsen, K.; Hu, S.J.; Carlson, B.E. Joining of dissimilar materials. *CIRP Ann.-Manuf. Technol.* **2015**, *64*, 526–533. [CrossRef]
3. Chen, Y.C.; Nakata, K. Microstructural characterization and mechanical properties in friction stir welding of aluminum and titanium dissimilar alloys. *Mater. Des.* **2009**, *30*, 469–474. [CrossRef]
4. Zhang, C.Q.; Robson, J.D.; Prangnell, P.B. Dissimilar ultrasonic spot welding of aerospace aluminum alloy AA2139 to titanium alloy TiAl6V4. *J. Mater. Process. Technol.* **2016**, *231*, 382–388. [CrossRef]
5. Tao, B.H.; Li, Q.; Zhang, Y.H.; Zhang, T.C.; Liu, Y. Effects of post-weld heat treatment on fracture toughness of linear friction welded joint for dissimilar titanium alloys. *Mater. Sci. Eng. A* **2015**, *634*, 141–146. [CrossRef]
6. Zhao, P.; Fu, L.; Chen, H. Low cycle fatigue properties of linear friction welded joint of TC11 and TC17 titanium alloys. *J. Alloy. Compd.* **2016**, *675*, 248–256. [CrossRef]
7. Xu, C.; Sheng, G.; Wang, H.; Feng, K.; Yuan, X. Tungsten Inert Gas Welding-Brazing of AZ31B Magnesium Alloy to TC4 Titanium alloy. *J. Mater. Process. Technol.* **2016**, *32*, 167–171. [CrossRef]
8. Wang, S.Q.; Li, W.Y.; Zhou, Y.; Li, X.; Chen, D.L. Tensile and fatigue behavior of electron beam welded dissimilar joints of Ti-6Al-4V and IMI834 titanium alloys. *Mater. Sci. Eng. A* **2016**, *649*, 146–152. [CrossRef]
9. Vairis, A.; Frost, M. High frequency linear friction welding of a titanium alloy. *Wear* **1998**, *217*, 117–131. [CrossRef]

10. Guo, Y.; Chiu, Y.; Attallah, M.M.; Li, H.; Bray, S.; Bowen, P. Characterization of Dissimilar Linear Friction Welds of α-β Titanium Alloys. *J. Mater. Eng. Perform.* **2012**, *21*, 770–776. [CrossRef]
11. Wanjara, P.; Jahazi, M. Linear friction welding of Ti-6Al-4V: Processing, microstructure, and mechanical-property inter-relationships. *Metall. Mater. Trans. A* **2005**, *36*, 2148–2164. [CrossRef]
12. Li, W.Y.; Ma, T.J.; Yang, S.Q. Microstructure evolution and mechanical properties of linear friction welded Ti-5Al-2Sn-2Zr-4Mo-4Cr (Ti17) titanium alloy joints. *Adv. Eng. Mater.* **2010**, *12*, 35–43. [CrossRef]
13. Ma, T.; Yan, M.; Yang, X.; Li, W.; Chao, Y.J. Microstructure evolution in a single crystal nickel-based superalloy joint by linear friction welding. *Mater. Des.* **2015**, *85*, 613–617. [CrossRef]
14. Chamanfar, A.; Jahazi, M.; Gholipour, J.; Wanjara, P.; Yue, S. Analysis of integrity and microstructure of linear friction welded Waspaloy. *Mater. Charact.* **2015**, *104*, 148–161. [CrossRef]
15. Astarita, A.; Curioni, M.; Squillace, A.; Zhou, X.; Bellucci, F.; Thompson, G.E.; Beamish, K.A. Corrosion behaviour of stainless steel-titanium alloy linear friction welded joints: Galvanic coupling. *Mater. Corros.* **2015**, *66*, 111–117. [CrossRef]
16. Grujicic, M.; Yavari, R.; Snipes, J.S.; Ramaswami, S. A linear friction welding process model for Carpenter Custom 465 precipitation-hardened martensitic stainless steel: A weld microstructure-evolution analysis. *J. Eng. Manuf.* **2015**, *228*, 1887–2020. [CrossRef]
17. Rotundo, F.; Marconi, A.; Morri, A.; Ceschini, A. Dissimilar linear friction welding between a SiC particle reinforced aluminum composite and a monolithic aluminum alloy: Microstructural, tensile and fatigue properties. *Mater. Sci. Eng. A* **2013**, *558*, 852–860. [CrossRef]
18. Bhamji, I.; Moat, R.J.; Preuss, M.; Threadgill, P.L.; Addison, A.C. Linear friction welding of aluminium to copper. *Sci. Technol. Weld. Join.* **2012**, *17*, 314–320. [CrossRef]
19. Bhamji, I.; Preuss, M.; Moat, R.J.; Threadgill, P.L.; Addison, A.C. Linear friction welding of aluminium to magnesium. *Sci. Technol. Weld. Join.* **2012**, *17*, 368–374. [CrossRef]
20. Ma, T.J.; Zhong, B.; Li, W.-Y.; Zhang, Y.; Yang, S.Q.; Yang, C.L. On microstructure and mechanical properties of linear friction welded dissimilar Ti-6Al-4V and Ti-6.5Al-3.5Mo-1.5Zr-0.3Si joint. *Sci. Technol. Weld. Join.* **2012**, *17*, 9–12. [CrossRef]
21. Wen, G.D.; Ma, T.J.; Li, W.Y.; Wang, S.Q.; Guo, H.Z.; Chen, D.L. Strain-controlled fatigue properties of linear friction welded dissimilar joints between Ti-6Al-4V and Ti-6.5Al-3.5Mo-1.5Zr-0.3Si alloys. *Mater. Sci. Eng. A* **2014**, *612*, 80–88. [CrossRef]
22. Zhao, P.; Fu, L. Strain hardening behavior of linear friction welded joints between TC11 and TC17 dissimilar titanium alloys. *Mater. Sci. Eng. A* **2015**, *621*, 149–156. [CrossRef]
23. Frankel, P.; Preuss, M.; Steuwer, A.; Withers, P.J.; Bray, S. Comparison of residual stresses in Ti-6Al-4V and Ti-6Al-2Sn-4Zr-2Mo linear friction welds. *Mater. Sci. Technol.* **2009**, *25*, 640–650. [CrossRef]
24. Karadge, M.; Preuss, M.; Lovell, C.; Withers, P.J.; Bray, S. Texture development in Ti-6Al-4V linear friction welds. *Mater. Sci. Eng. A* **2007**, *458*, 182–181. [CrossRef]
25. Lang, B.; Zhang, T.C.; Li, X.H.; Guo, D.L. Microstructural evolution of a TC11 titanium alloy during linear friction welding. *J. Mater. Sci.* **2010**, *45*, 6218–6224. [CrossRef]
26. Romero, J.; Attallah, M.M.; Preuss, M.; Karadge, M.; Bray, S.E. Effect of the forging pressure on the microstructure and residual stress development in Ti-6Al-4V linear friction welds. *Acta Mater.* **2008**, *57*, 5582–5592. [CrossRef]
27. Corzo, V.; Casals, O.; Alcalá, J.; Mateo, A.; Anglada, M. Mechanical evaluation of linear friction welds in titanium alloys through indentation experiments. *Weld. Int.* **2007**, *21*, 125–128. [CrossRef]
28. Schroeder, F.; Ward, R.M.; Turner, R.P.; Walpole, A.R.; Attallah, M.M.; Gebelin, J.-C.; Reed, R.C. Validation of a Model of Linear Friction Welding of Ti6Al4V by Considering Welds of Different Sizes. *Metall. Mater. Trans. B* **2015**, *46*, 2326–2331. [CrossRef]
29. Turner, R.; Gebelin, J.-C.; Ward, R.M.; Reed, R.C. Linear friction welding of Ti-6Al-4V: Modelling and validation. *Acta Mater.* **2011**, *59*, 3792–3803. [CrossRef]
30. McAndrew, A.R.; Colegrove, P.A.; Addison, A.C.; Flipo, B.C.D.; Russell, M.J. Modelling the influence of the process inputs on the removal of surface contaminants from Ti-6Al-4V linear friction welds. *Mater. Des.* **2015**, *66*, 183–195. [CrossRef]
31. Grujicic, M.; Arakere, G.; Pandurangan, B.; Yen, C.-F.; Cheeseman, B.A. Process Modeling of Ti-6Al-4V Linear Friction Welding (LFW). *J. Mater. Eng. Perform.* **2012**, *21*, 2011–2023. [CrossRef]

32. Ma, T.; Chen, T.; Li, W.-Y.; Wang, S.; Yang, S. Formation mechanism of linear friction welded Ti-6Al-4V alloy joint based on microstructure observation. *Mater. Charact.* **2011**, *62*, 130–135. [CrossRef]
33. Ji, Y.; Chai, Z.; Zhao, D.; Wu, S. Linear friction welding of Ti-5Al-2Sn-2Zr-4Mo-4Cr alloy with dissimilar microstructure. *J. Mater. Process. Technol.* **2014**, *214*, 878–887. [CrossRef]
34. Zhao, P.K.; Fu, L.; Zhong, D.C. Numerical simulation of transient temperature and axial deformation during linear friction welding between TC11 and TC17 titanium alloys. *Comput. Mater. Sci.* **2014**, *82*, 325–333. [CrossRef]
35. Ma, T.J.; Li, W.-Y.; Yang, S.Y. Impact toughness and fracture analysis of linear friction welded Ti-6Al-4V alloy joints. *Mater. Des.* **2008**, *30*, 2128–2132. [CrossRef]
36. Ji, Y.; Wu, S. Study on microstructure and mechanical behavior of dissimilar Ti17 friction welds. *Mater. Sci. Eng. A* **2014**, *586*, 32–40. [CrossRef]